

# Permeability Modeling for SAGD Using Mini-Models

Jason McLennan\*, Clayton V. Deutsch\*, David Garner\*\*, T.J. Wheeler\*\*,  
Jean-François Richy\*\*\*, and Emmanuel Mus\*\*\*

\*Centre for Computational Geostatistics, University of Alberta

\*\*ConocoPhillips Canada, Calgary, Canada

\*\*\*Total, seconded to ConocoPhillips Canada, Calgary, Canada

*The predicted flow performance of Steam Assisted Gravity Drainage (SAGD) well pairs is sensitive to the spatial distribution of permeability. Permeability measurements taken from small scale core data are often both limited and biased. Mini-models of porosity and permeability are constructed and flow simulated in order to establish representative relationships/correlations at the grid block scale used in SAGD flow simulation. The mini-models are constructed on a by-facies basis honoring the spatial variability within each category. The uncorrected mini-model flow results lead to a too narrow range of permeability. Geostatistical scaling laws are applied to correct the permeability values. This paper presents a permeability modeling and debiasing procedure with application to the McMurray Oilsands SAGD reservoir on the Surmont Lease in Northern Alberta, Canada. The mini-model construction, flow simulation of the mini-models, and derivation of representative porosity/permeability statistics are all described and documented in this context. A comparison of SAGD flow simulation results (recovered bitumen and steam-oil-ratio) with different permeability modeling procedures is presented to support the relative importance of the chosen method.*

## Introduction

The thermal SAGD process, invented by Dr. Roger Butler in 1978 [1,2] for in-situ heavy oil recovery, is now well accepted and understood. Steam is injected in an upper injection well to lower the viscosity of surrounding oil allowing it to drain along a growing cone-shaped steam chamber into a lower production well via gravity. The acceptance of SAGD drives Canada to second (after only Saudi Arabia) on a world list of proven reserves with some 175 billion barrels [3]. Moreover, roughly 40 major Albertan oilsands projects are underway or planned with an expected yield of 1.8 million barrels per day by 2010 [4].

The most powerful instrument available for forecasting reservoir performance is flow simulation. Modern flow simulators such as CMG *STARS* [5] are capable of modeling, in addition to conventional three-phase fluid flow, the transfer of heat from steam to the surrounding reservoir. Thermal simulators of this type can be used to quantify SAGD production performance. The SAGD production performance parameters considered in this work are cumulative oil production (COP), instantaneous oil rate (IOR), cumulative steam-oil-ratio (CSOR), and cumulative water injection (CWI).

Several reservoir parameters and their associated uncertainties impact the inference of SAGD production. Of all such geological, engineering, flow simulation, and economic parameters, the inherently uncertain spatial distribution of petrophysical properties is perhaps the most important [6]. Different distributions of one or all of facies type, porosity, water/oil/gas saturation, and permeability certainly have a significant effect on all of COP, IOR, CSOR, and CWI. And out of

all these petrophysical properties, permeability is likely the single most important variable. The subject of this paper is focused on constructing robust permeability models for SAGD flow simulation.

### Permeability Modeling

The traditional method for modeling permeability is with linear or quadratic by-facies porosity-permeability correlations using core measurements [7]. These correlations are used to transform interpolated log porosity to permeability at the geological model scale. The permeability is then downscaled for SAGD flow simulation [8]. Although this methodology is straightforward, there are some practical challenges and limitations:

1. Seldom are there sufficient core permeability measurements to reliably infer the by-facies porosity-permeability relationships due to significant time and economic costs of collecting core permeability data [9]. Moreover, the available porosity-permeability pairs are often quite random and difficult to fit with a simple linear or quadratic function.
2. Oilsands core porosity and permeability measurements are optimistically biased due to expansion of the core after extraction and rising to the surface. This bias can then be compounded with preferentially sampling for clean and well behaved intervals [10].
3. The differences in scale from small core samples where the porosity-permeability relationships are established to the larger geological property modeling grid where the porosity and permeability are interpolated to the intermediate SAGD flow simulation grid where the porosity and permeability are used to calculate production performance are often ignored in practice for simplicity.

There are several available procedures aimed at overcoming the challenges above. Most methodologies are straightforward, but fall short of accounting for all three issues. An excellent state-of-the-art methodology that addressed all three issues simultaneously is presented and applied by Waite et al. [11] for the Hamaca Field within the Orinoco Heavy Oil Belt of Venezuela. This work provides an alternative method that is straightforward and robust.

The proposed permeability modeling methodology accounts for limited and naturally random permeability data, core expansion and preferential sampling, as well as the scale differences between core, geological grid cell volumes, and flow simulation grid cell volumes. Furthermore, the procedure is efficient, can be largely automated, and is robust for various heavy oil applications. The proposed permeability modeling methodology is applied to the Surmont SAGD reservoir. The resulting permeability model is downscaled to the flow simulation grid and flow simulations for a single well pair model are conducted. The resulting COP, IOR, CSOR, and CWI production performance measures are then compared to the results using a traditional permeability model from simple by-facies quadratic relationships.

The methodology can be summarized in two overall major steps. The first step involves debiasing and re-scaling the by-facies core horizontal permeability  $k_H$  versus porosity  $\phi$  relationships using mini-models. This step involves seven working phases, addresses all three issues above simultaneously, and constitutes the majority of the entire process. The second step is modeling permeability on the geological grid using a combined probability field cloud transformation technique. This step exploits the representative distributions established in the first step and is relatively fast. These two steps are first described in general and then described in all necessary detail.

## Overview of Proposed Methodology

The two key features of the methodology are (1) the integration of lower porosity or increased *shaliness* into measurements from dilated and preferentially sampled core and (2) the translation of porosity-permeability relationships at the core scale to the SAGD flow simulation scale. The proposed methodology does not require large core databases.

A representative  $1.0 \times 1.0 \times 0.5\text{m}^3$  ( $0.5\text{m}^3$ ) mini-model roughly the size of a typical flow simulation grid cell are utilized as miniature numerical laboratories to infer the debiased by-facies  $k_H$ - $\phi$  relationships at the flow simulation scale. Figure 1 (left) shows a typical schematic mini-model. A fine-scale grid network at roughly the core scale is tabulated in Figure 1 (right). There are a total of 62,500 cells measuring 0.02m (2cm) on each side for an  $8.0\text{cm}^3$  grid cell volume. All phases of work in the first step of the methodology are performed within this mini-model setup.

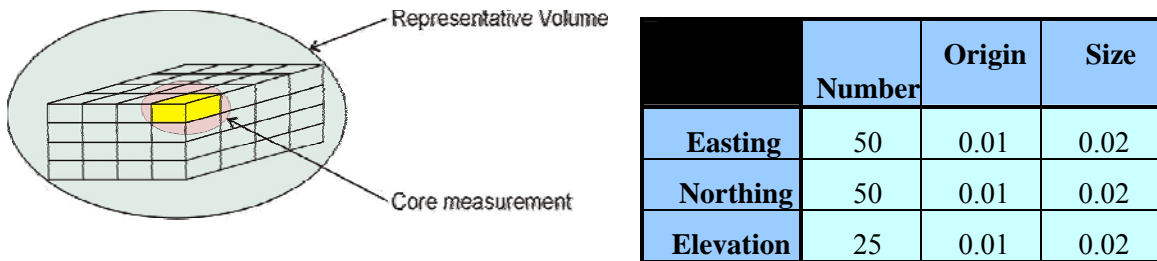


**Figure 1** – A schematic mini-model (left) and tabulated grid system (right).

The spatial distributions of porosity within the mini-models are visually calibrated to core photos showing representative McMurray shale heterogeneity within each facies. The by-facies porosity minimum and maximum limits are derived from logging measurements from which representative  $k_H$  and  $k_V$  distributions can be calibrated. These resulting by-facies permeability distributions are input into a simple steady-state single phase flow simulator to calculate effective horizontal and vertical permeabilities at the subsequent SAGD flow simulation scale. This is repeated multiple times within each facies so that a reliable scatter of  $k_H$ - $\phi$  pairs can be constructed even with limited core data. The resulting representative  $k_H$  versus  $\phi$  distributions are adjusted using volume variance theory so that they will accurately reflect the anticipated permeability uncertainty.

It is important to emphasize the core porosity values do not change – the log porosity limits are simply used to extend its relationship to permeability to unbiased limits. This ensures that lower horizontal and vertical permeabilities are represented fairly.

## Surmont Application

The  $k_H$  and  $k_V$  permeabilities are modeled within the blue outlined area in Figure 2 (left). The grid network is also shown (right). There are 20 geostatistical realizations of facies, porosity, and water saturation previously constructed and available on the same grid.

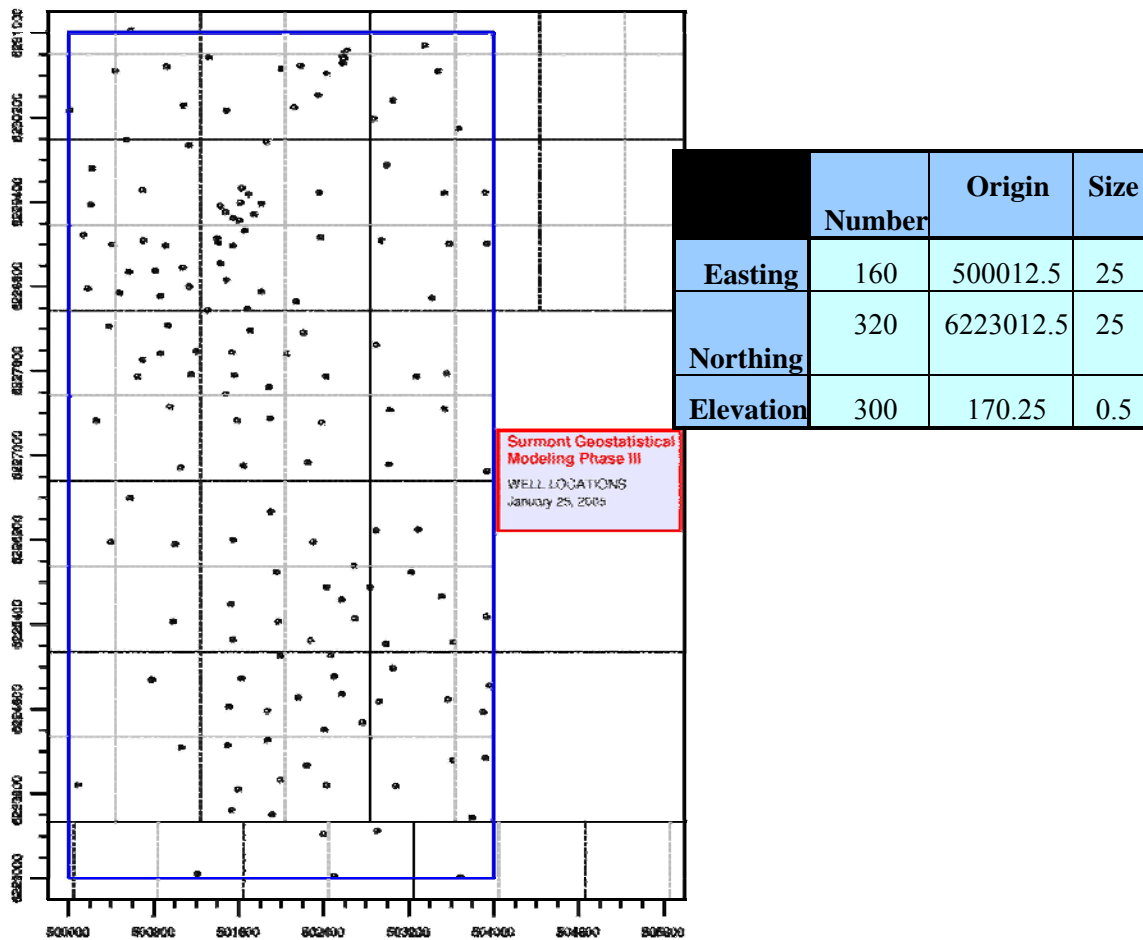


**Figure 2** – An illustration of the domain (blue outline - left) and grid (right) for geological modeling.

There are a total of 157 wells with log facies and porosity measurements available within the model area in Figure 2. There are a total of 35 wells with core facies,  $\phi$ ,  $k_H$ , and  $k_V$  measurements available over the entire Surmont Lease with only fourteen located inside the model area. Nonetheless, all 760 collocated measurements from all 35 wells are used in the subsequent permeability modeling procedure. Five facies types are considered: (1) sand (*SC*), (2) breccia (*BRC*), (3) sandy inclined heterolithic strata (*SIHS*), (4) muddy inclined heterolithic strata (*MIHS*), and (5) shale (*SH*). Of the 760 total core measurements, 473, 53, 146, 50, and 38 are collocated with, in order, *SC*, *BRC*, *SIHS*, *MIHS*, and *SH* facies.

Three sets of permeability related cross plots for all 760 data are shown in Figure 3:  $k_H$  (core) vs  $\phi$  (core),  $k_V$  (core) vs  $k_H$  (core), and  $\phi$  (log) vs  $\phi$  (core). The correlations are 0.618, 0.899, and 0.450, respectively. Figure 4 shows the  $k_H$  (core) vs  $\phi$  (core) scatters by-facies for *BRC*, *SIHS*, and *MIHS*. The correlations here are 0.834, 0.654, and 0.507, respectively. The optimistic core bias is apparent in all of the bivariate scatters in Figures 3 and 4. The core  $\phi$  measurements are indeed systematically higher than the log  $\phi$  measurements; and since  $k_H$  and  $\phi$  are well correlated,  $k_H$  and  $k_V$  are also biased too high. These by-facies biased  $k_H$  and  $k_V$  univariate distributions are shown in Figure 5.

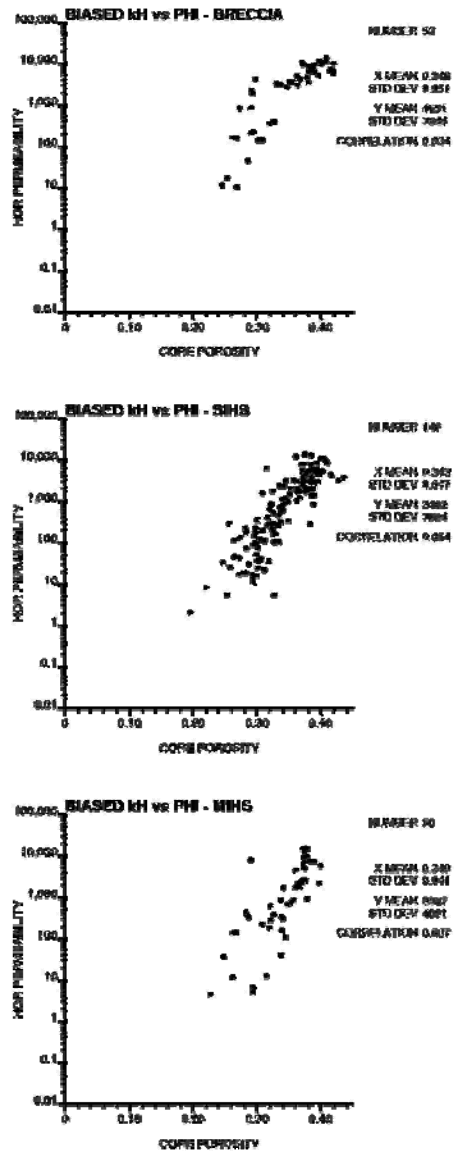


Figure 3 – Scatter of  $k_H$ -  $\phi$  (core),  $k_V$ - $k_H$ , and  $\phi$  (log)-  $\phi$  (core) using all 760 core data

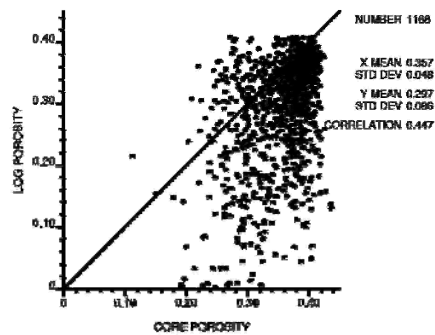
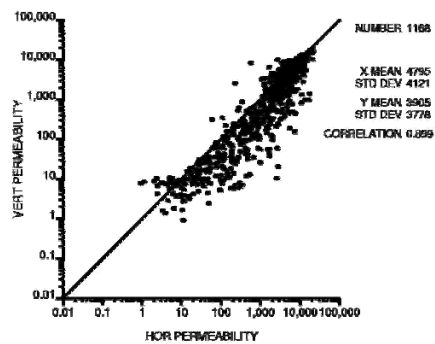
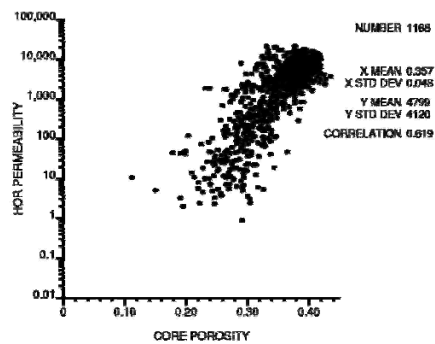


Figure 4 – Scatter of  $k_H$ -  $\phi$  (core) within the *BRC*, *SIHS*, and *MIHS* facies.

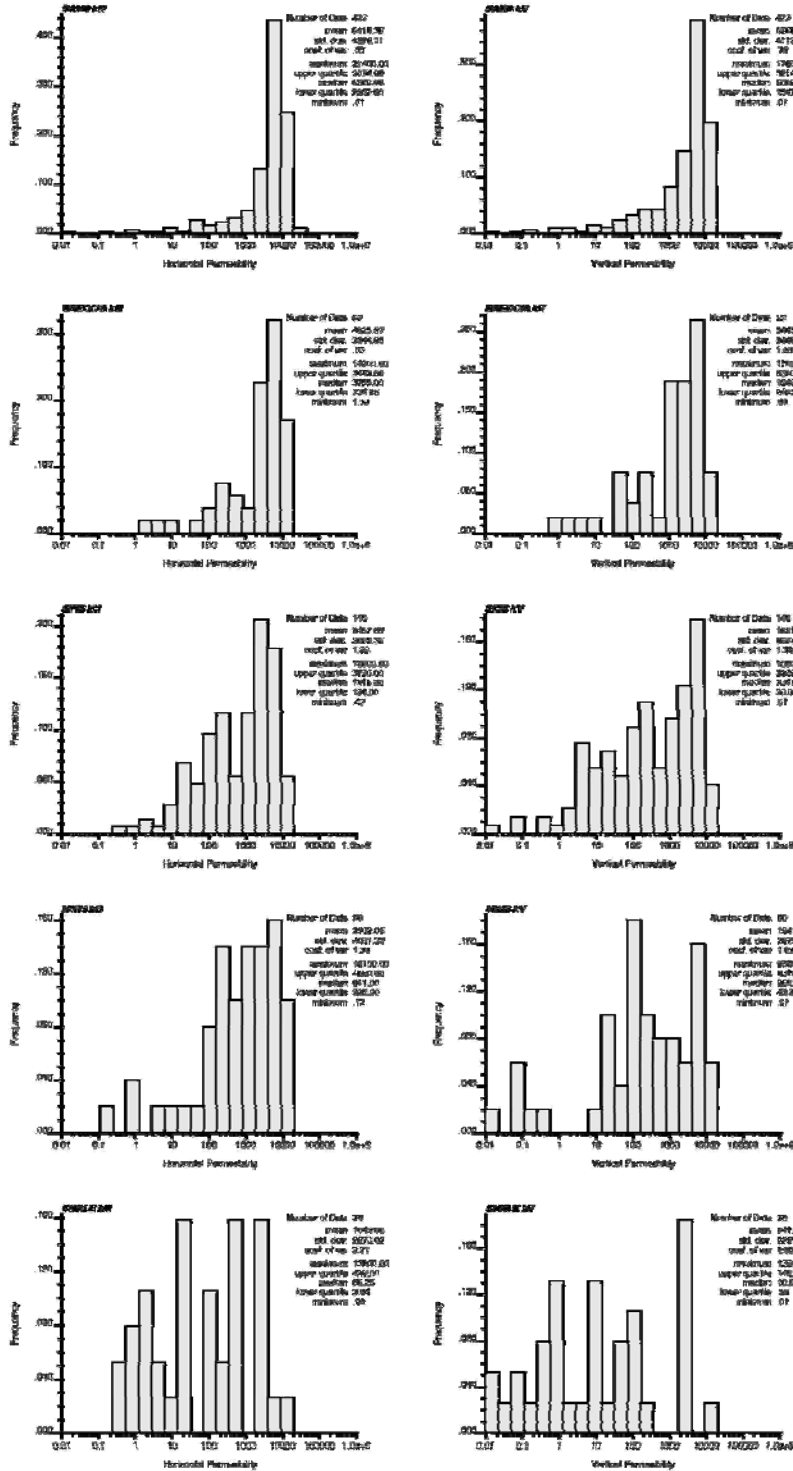


Figure 5: The biased by-facies histograms of  $k_H$  and  $k_V$  using the 760 collocated core data.

All necessary detail of the proposed permeability modeling method is now presented. Recall there are two major steps and seven phases to the longer first step. The figures and illustrations are shown for the *BRC*, *SIHS*, and *MIHS* facies during the description.

### Step One: $k_H$ - $\phi$ Correlations

The bivariate  $k_H$  vs  $\phi$  relationships are first established using the mini-model approach. There are seven phases to this first step of the permeability modeling methodology. The first step is to simulate  $V_{\text{shale}}$ .

The volume fraction of shale  $V_{\text{SHALE}}$  is simulated using sequential Gaussian simulation. The spatial correlation or variogram is visually calibrated to core photos representative of typical McMurray Formation heterogeneity from the Surmont lease. The unconditionally simulated Gaussian values are then converted to a lognormal  $V_{\text{SHALE}}$  distribution with randomly drawn mean between 0 and 100% and standard deviation of 20%. Figure 1 illustrates the consistency between some typical core photos and the resulting mini-model shale heterogeneity for the *BRC*, *SIHS*, and *MIHS* facies.

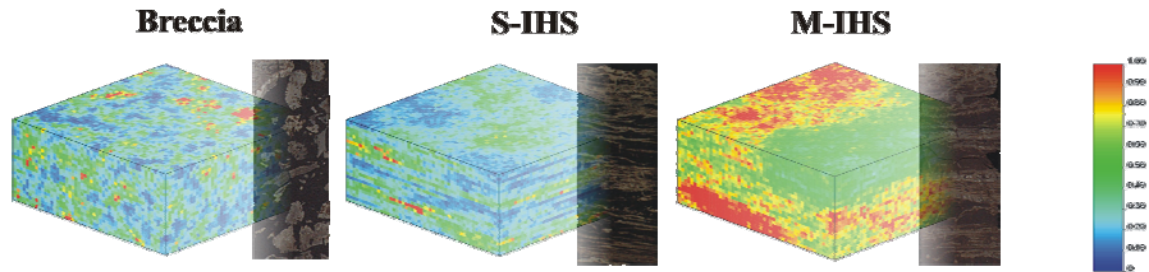


**Figure 5:** Comparison of core photos to the visually calibrated mini-model shale heterogeneity.

The use of  $V_{\text{SHALE}}$  could be confusing. We are not directly using any  $V_{\text{SHALE}}$  data;  $V_{\text{SHALE}}$  is a surrogate variable that provides a mechanism to create models with lower porosity than observed in the core data. This permits us to fill in the entire distribution of fair porosity values. An obvious area of future work is the quantification of the spatial correlation using the  $V_{\text{SHALE}}$  data directly and comparison to these results.

*Convert  $V_{\text{SHALE}}$  to  $\phi$*

The following relationship is used to convert the  $V_{\text{SHALE}}$  models to  $\phi$ :

$$\phi = (1 - V_{\text{SHALE}}) \phi_{\text{NET}} + V_{\text{SHALE}} \cdot \phi_{\text{NON-NET}} \quad (1)$$

where  $\phi_{\text{NET}}$  and  $\phi_{\text{NON-NET}}$  are the maximum and minimum by-facies log porosity values, respectively. These values are listed by-facies in Table 1. Formula (1) ensures the fair full range of possible porosity is accounted for. An important assumption is that the extreme log porosity values are unbiased and reasonably represent the true extreme porosities. The missing shale or low porosity reservoir material is effectively injected into the by-facies geological mini-models.

| Representative Log Porosity Limits   |           |            |             |             |           |
|--------------------------------------|-----------|------------|-------------|-------------|-----------|
|                                      | <i>SC</i> | <i>BRC</i> | <i>SIHS</i> | <i>MIHS</i> | <i>SH</i> |
| $\square_{NET}$                      | 0.00      | 0.06       | 0.02        | 0.00        | 0.00      |
| $\square\square\square\square_{NET}$ | 0.40      | 0.37       | 0.39        | 0.35        | 0.36      |

**Table 1:** The fair porosity limits taken from the extreme log porosity values.

Figures 6 and 7 show the simulated  $V_{SHALE}$  and representative  $\phi$  distributions for a typical mini-model run. Notice the presence now of more realistic lower porosity. The resulting representative distributions of  $\phi$  are used in subsequent phases to create representative  $k_H$  and  $k_V$  distributions.

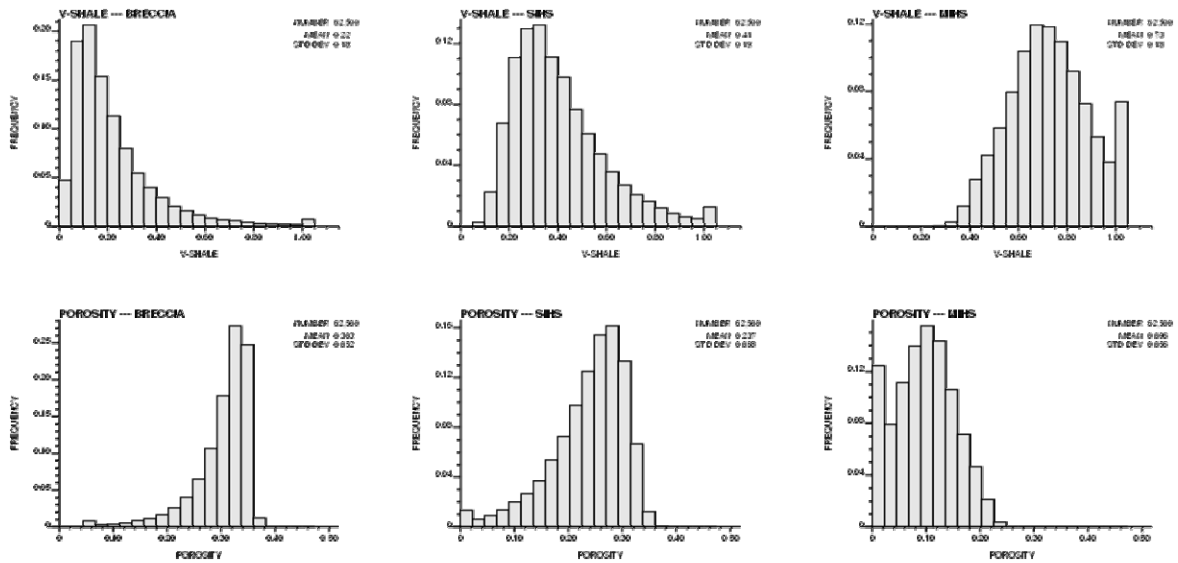


**Figure 6:** The  $V_{SHALE}$  and corrected  $\phi$  distributions for a typical mini-model run.

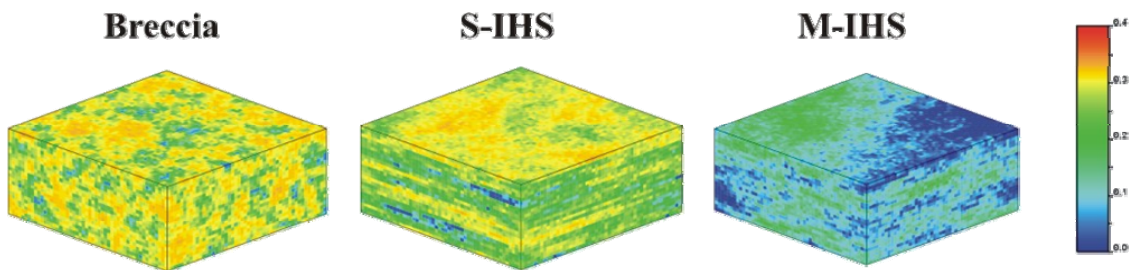


**Figure 7:** The spatial distribution of a corrected  $\phi$  distribution for a typical mini-model run.

### Representative $k_H$ - $\phi$ Relationship

This phase merges the  $k_H$ - $\phi$  correlation from core measurements with the representative porosity distributions calculated in the previous phase to calculate new representative  $k_H$ - $\phi$  bivariate

distributions. A GSLIB [12]-like program named *bimodel* is used for this merging and calibration process. The program quantifies a bivariate distribution at a user-defined discretization in  $k_H$  and  $\phi$ . Here, the horizontal  $\phi$  axis has 45 bins from 0 to 45% and the vertical  $k_H$  axis has 50 bins from 0.001 to 15,000mD for a total of 2,250 unbiased 2D bivariate discretization points to identify.

A number of options are available for establishing the representative  $k_H$  vs  $\phi$  distributions. The raw  $k_H$ -  $\phi$  data can be grouped according to the representative  $\phi$  distribution axis bins; in this case, the conditional cumulative distribution functions (ccdfs) are calculated numerically. Initially, this option was implemented; however, the resulting distributions were too erratic due to the low number of raw by-facies data and their preferential high porosity and permeability densities. Another option is to assume that the raw bivariate  $k_H$  vs  $\phi$  scatters are approximately bivariate normal and fully parameterized by the  $k_H$  and  $\phi$  mean and  $k_H$ -  $\phi$  correlation coefficient. Under this assumption, the set of 45 representative  $k_H$  ccdfs can be calculated analytically. This option is finally implemented due to its robust results compared to using the raw core data.

The representative  $k_H$  vs  $\phi$  bivariate distributions are shown in Figure 8. The color scale represents the ccdf values from 0 (blue) to 1 (red). At each of the previously defined 45 representative porosity bins, a cross section through this plot reveals the Gaussian ccdf for horizontal permeability  $k_H$ . These representative bivariate  $k_H$  vs  $\phi$  distributions are used in the next phase to generate representative  $k_H$  and  $k_V$  distributions at the mini-model scale.

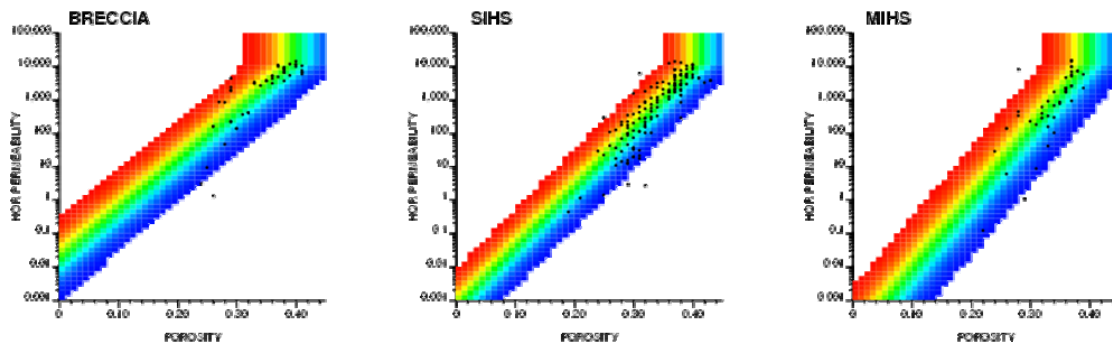


**Figure 8:** The representative bivariate  $k_H$  vs  $\phi$  distributions over all scales.

#### Representative $k_H$

This stage simulates from the representative  $k_H$  vs  $\phi$  bivariate distributions generated in the previous phase according to a correlated probability field and the representative porosity distributions constructed in the second phase in order to create unbiased  $k_H$  mini-models for subsequent flow simulation. A GSLIB environment program named *cltrans* implements the combined probability field cloud transformation. The required inputs are correlated probability fields, the representative  $\phi$  distributions calculated in the second phase, and the bivariate  $k_H$  vs  $\phi$  distributions calculated in the previous phase.

A correlated probability field is simulated over the mini-model grid cells using sequential Gaussian simulation with a 0% nugget and isotropic 30cm range variogram within each facies. At each of the 62,500 mini-model cells, a representative porosity value  $\phi$  (from the second phase) and probability value  $p$  is then available. The representative  $k_H$  value is then simulated as the  $p$ -quantile of the appropriate  $k_H$  ccdf in the previous phase. Some typical representative  $k_H$

distributions resulting from this process are shown in Figure 9. Notice the lower  $k_H$  frequencies previously unavailable without the mini-model approach.

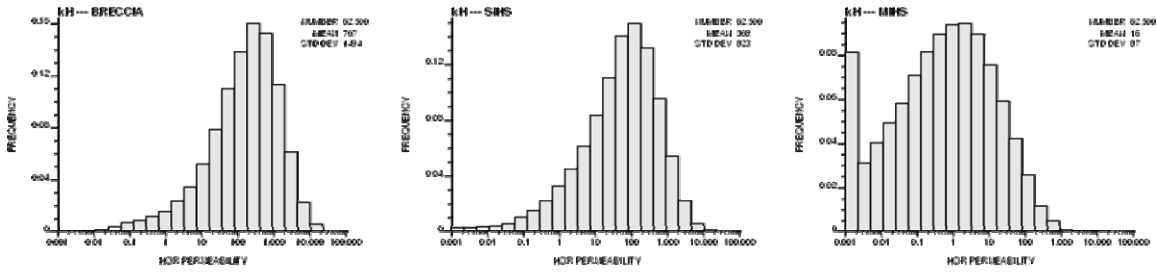


**Figure 9:** The representative univariate  $k_H$  distributions at the mini-model scale.

The combined probability field cloud transformation is the essential technique used in the second step of the overall permeability modeling methodology. The reason for using this particular transformation as well as additional implementation details are provided there.

*Representative  $k_V$*

The approach for calculating  $k_V$  at the mini-model and geological scale is through the 760  $k_V:k_H$  ratio data available from core measurements. The  $k_V:k_H$  ratio is first simulated within the mini-model grid using a 10% nugget and isotropic 30cm range variogram and the by-facies reference distributions of core-derived  $k_V:k_H$  ratios. The maximum allowed  $k_V:k_H$  ratio is 1. At each of the 62,500 mini-model grid cells, the representative  $k_V$  value is then simply calculated as the  $k_V:k_H$  ratio value multiplied by the corresponding  $k_H$  value simulated in the previous phase. Some typical  $k_V:k_H$  ratio models and representative  $k_H$  distributions resulting from the multiplication are shown in Figure 10. Notice again the lower  $k_V$  frequencies previously unavailable without the mini-model approach.

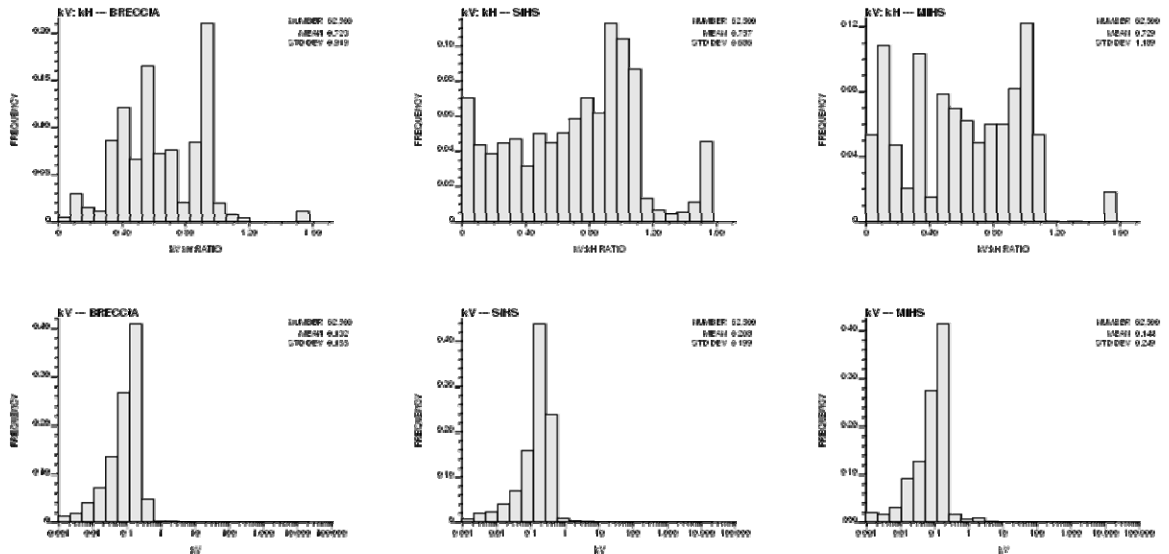


**Figure 10:** The representative univariate  $k_H$  distributions at the mini-model scale.

*Representative  $k_H$ -  $\phi$  Scatter*

A steady-state single phase flow simulation is implemented to calculate the effective horizontal flow rates and the corresponding effective horizontal permeabilities  $k_H$  through Darcy’s Law. The effective porosity  $\phi$  is also calculated with a simple arithmetic average. Repeating the previous phases up until now a total of 250 times within each facies, representative  $k_H$  vs  $\phi$  bivariate scatters that account for sampling bias and diverse scales can be constructed. Figure 11 shows the results. The solid red line represents conditional expectation curves from the third phase – the results are consistent.

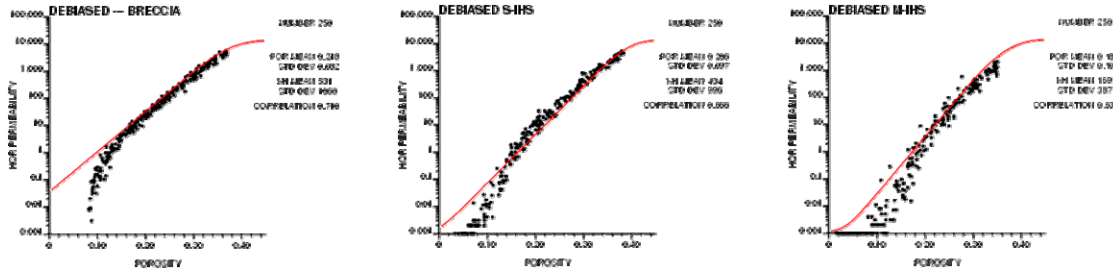


**Figure 11:** The representative bivariate  $k_H$  vs  $\phi$  distributions for the flow simulation scale.

*Variance Inflation*

This last phase is needed in order to exploit the representative relationships developed in the previous phase. The effective  $k_H$  values from the steady state flow simulation average out geological variability quickly resulting in the narrow  $k_H$  cdfs in Figure 11. This presents a problem in practice since these too tight correlations will underestimate the true uncertainty in  $k_H$ . There is a need then to inflate the conditional distribution variances in order for the true permeability heterogeneity to be captured. A variance inflation factor (*VIF*) is calculated in this capacity using geostatistical scaling laws from the mini-model to model area dispersion variances.

The *VIF* calculation involves several steps. All of the calculations are performed within each facies separately. The results are summarized in Table 2.

| Variance Inflation Factor Calculation  |        |                       |                          |             |                    |            |
|--|--------|-----------------------|--------------------------|-------------|--------------------|------------|
|  | $\rho$ | $D^2_{(CORE-MA2005)}$ | $\sim D^2_{(MM-MA2005)}$ | $\rho(v,v)$ | $D^2_{(V-MA2005)}$ | <i>VIF</i> |
| <i>SC</i>  | 0.06   | 0.799623              | 0.095044                 | 0.334       | 0.533              | 5.603      |
| <i>BRC</i>   | 0.00   | 0.357999              | 0.059804                 | 0.429       | 0.204              | 3.418      |
| <i>SIHS</i>  | 0.00   | 0.453394              | 0.152053                 | 0.416       | 0.265              | 1.741      |
| <i>MIHS</i>  | -0.26  | 0.711314              | 0.243210                 | 0.356       | 0.458              | 1.884      |
| <i>SH</i>  | -0.47  | 0.433481              | 0.262206                 | 0.200       | 0.347              | 1.323      |
| <i>V</i> = 25 x 25 x 1m ----- Easting, Northing, Elevation<br><i>MM</i> = 1 x 1 x 0.5m ----- Easting, Northing, Elevation<br><i>MA2005</i> = 4000 x 8000 x 320m ----- Easting, Northing, Elevation<br><i>CORE</i> = 0.10 x 0.10m ----- Circumference, Height |        |                       |                          |             |                    |            |

**Table 2:** A summary of all the required prior quantities for the calculation of the *VIF* by-facies.

The first step is to calibrate the horizontal permeability power law averaging constant  $\phi$  by-facies. This is done using the 250 representative  $k_H$  mini-models from the fourth phase and the 250 effective  $k_H$  values from flow simulation in the previous (sixth) phase. The  $\phi$  constant is iterated on until the power averaging process of the  $k_H$  mini-model converges on the corresponding flow simulated effective  $k_H$  value. The average  $\phi$  power over all 250 runs is listed in Table 2. All of the subsequent dispersion variance calculations and manipulations are performed in power law space using the  $k_H^\omega$  data.

The maximum dispersion variance  $D^2_{(CORE,MA2005)}$  is required within each facies. This variance is calculated as the average variance taken over eight equally wide 5% porosity conditioning windows from 0 to 40%. These are listed in Table 2. The target variability at the geological modeling scale  $D^2_{(V,MA2005)}$  is then calculated as a portion of this maximum dispersion variance according to the following volume variance relationship by-facies:

$$D^2_{(V,MA2005)} = D^2_{(CORE,MA2005)} \left(1 - \overline{\gamma_{(V,V)}}\right) \quad (2)$$

The *gamma-bar* value is the last link to the target variability and *VIF*. This is calculated within each facies using the same porosity variograms as those used for the 3D geostatistical porosity modeling work. The resulting  $D^2_{(V,MA2005)}$  values are listed in Table 2. The *VIF* is then simply the ratio between the target variability  $D^2_{(V,MA2005)}$  and the average variability currently captured in the mini-models  $D^2_{(MM,MA2005)}$ :

$$VIF = \frac{D^2_{(V,MA2005)}}{D^2_{(MM,MA2005)}} \quad (3)$$

The  $D^2_{(MM,MA2005)}$  dispersion variance is calculated similarly to the maximum dispersion variance  $D^2_{(CORE,MA2005)}$ . The representative bivariate  $k_H$  vs  $\phi$  distributions from the previous phase are separated according to eight equally wide 5% porosity conditioning windows from 0 to 40%. The variance of  $k_H$  within each window is calculated and averaged to obtain the final  $D^2_{(MM,MA2005)}$  values listed in Table 2. And of course, the *VIF* factors are also listed in Table 2.

The same *VIF* factor is applied to the  $k_H$  cdf corresponding to each of the previously established 45 porosity bins (see the third phase) within each of the five facies types. This correction is applied using an affine correction. The resulting variance corrected  $k_H$  vs  $\phi$  bivariate distributions are shown in Figure 12. The red bullets represent the variance corrected  $k_H$ -  $\phi$  scatter of pairs. The original biased distributions in Figure 4 are shown with lightly shaded bullets. And a quadratic by-facies porosity-permeability regression relationship is shown with a solid blue line.

The corrected  $k_H$  vs  $\phi$  bivariate distributions (red) in Figure 12 provide the key link for subsequent permeability modeling at the geological scale and SAGD flow simulation modeling at the mini-model scale. These by-facies bivariate relationships effectively and efficiently account for core expansion and preferential core sampling as well as the difference in scale between core measurements, geological model grid cells, and flow simulation grid cells. The procedure also does not require significant time and resource costs associated with collecting numerous core permeability measurements.

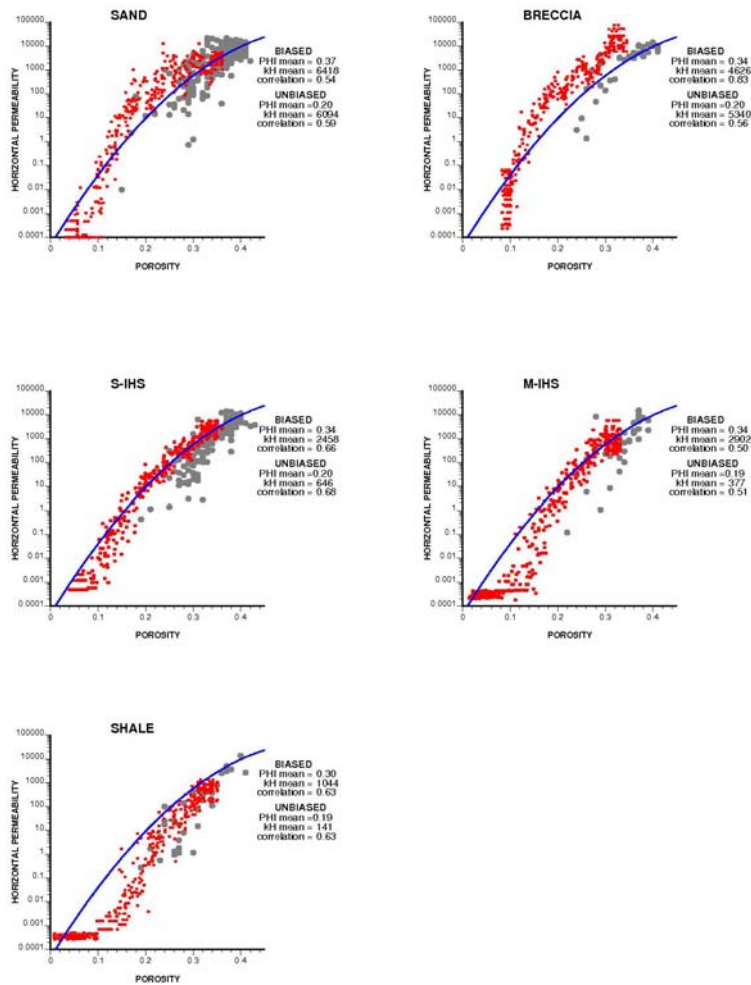


**Figure 12:** The by-facies representative variance corrected  $k_H$  vs  $\phi$  calibrations (red). The biased core data (shaded) and a quadratic permeability curve (blue) are also shown for reference.

### Step Two: Permeability Transform

The last step of the permeability modeling methodology is a combined probability field cloud transformation. This last step is performed at the geological modeling scale using the mini-model flow simulation scale calibrations in Figure 12. This step is relatively straightforward. In fact, the procedure is similar to that used in the fourth phase of the first step. The  $k_H$  variable is simulated from the representative  $k_H$  vs  $\phi$  bivariate distributions in Figure 12 according to a correlated probability field and the previously constructed porosity distributions at the geological modeling scale. In other words, the  $k_H$  realizations are spatially drawn from the  $k_H$  cdfs embedded within the representative  $k_H$  vs  $\phi$  bivariate distributions in Figure 12 corresponding to previously modeled collocated porosity values.

Using the representative  $k_H$  vs  $\phi$  bivariate by-facies distributions in Figure 12 for the cloud transformation ensures the resulting permeability models fairly represent lower permeabilities and increased shaliness that would have otherwise been ignored using core measurements alone.

These relationships also are applicable at the flow simulation scale, and reproduce the correct permeability dispersion variance. Furthermore, a large database of core permeability measurements was not required.

The cdf realizations are drawn according to a spatially correlated probability field in order to accurately represent the spatial variability of permeability as quantified by the variogram. Randomly drawing from the cdfs does not guarantee realistic permeability heterogeneity. Correlated probability fields are simulated using sequential Gaussian simulation. The by-facies calculated (points) and modeled (line) horizontal and vertical  $k_H$  variograms are shown in Figure 13. A vertical-to-horizontal anisotropy ratio was used to model the horizontal *SIHS* and *MIHS* variograms due to the sparse core data.

At each of the 15,360,000 25 x 25 x 0.5m geological grid cells, representative porosity values  $\phi$  from the previously available 3D modeling and probability values  $p$  from the probability field are available. The  $k_H$  value is taken as the  $p$ -quantile from the cdf that corresponds to the  $\phi$  value at each grid cell location. This is repeated for 20 realizations.

The  $k_V$  variable is modeled in a similar way to the fifth phase of the first overall step, that is, by previously simulating the  $k_V:k_H$  ratio and multiplying by  $k_H$ . A variography study of the  $k_V:k_H$  ratio indicates an almost pure isotropic nugget effect model. The  $k_V$  value is obtained from multiplying  $k_V:k_H$  by  $k_H$ . This is repeated for all 20 realizations.

Figures 13 and 14 show several cross sections through the first porosity and  $k_H$ , realization. The same cross section locations are used in each figure. The horizontal and vertical permeability is set to 0.001mD within shale facies. Notice the significant control that the porosity model in Figure 13 and by-facies  $k_H$  vs  $\phi$  bivariate correlations in Figure 12 has on permeability in Figure 14. Also notice the increased spatial variability in permeability relative to porosity. This variability could have been too large had a random cloud transform with no probability field been applied. On the contrary, the permeability variability may have been too low had the *VIF* not been applied.

The figure showing vertical permeability was removed to save space.

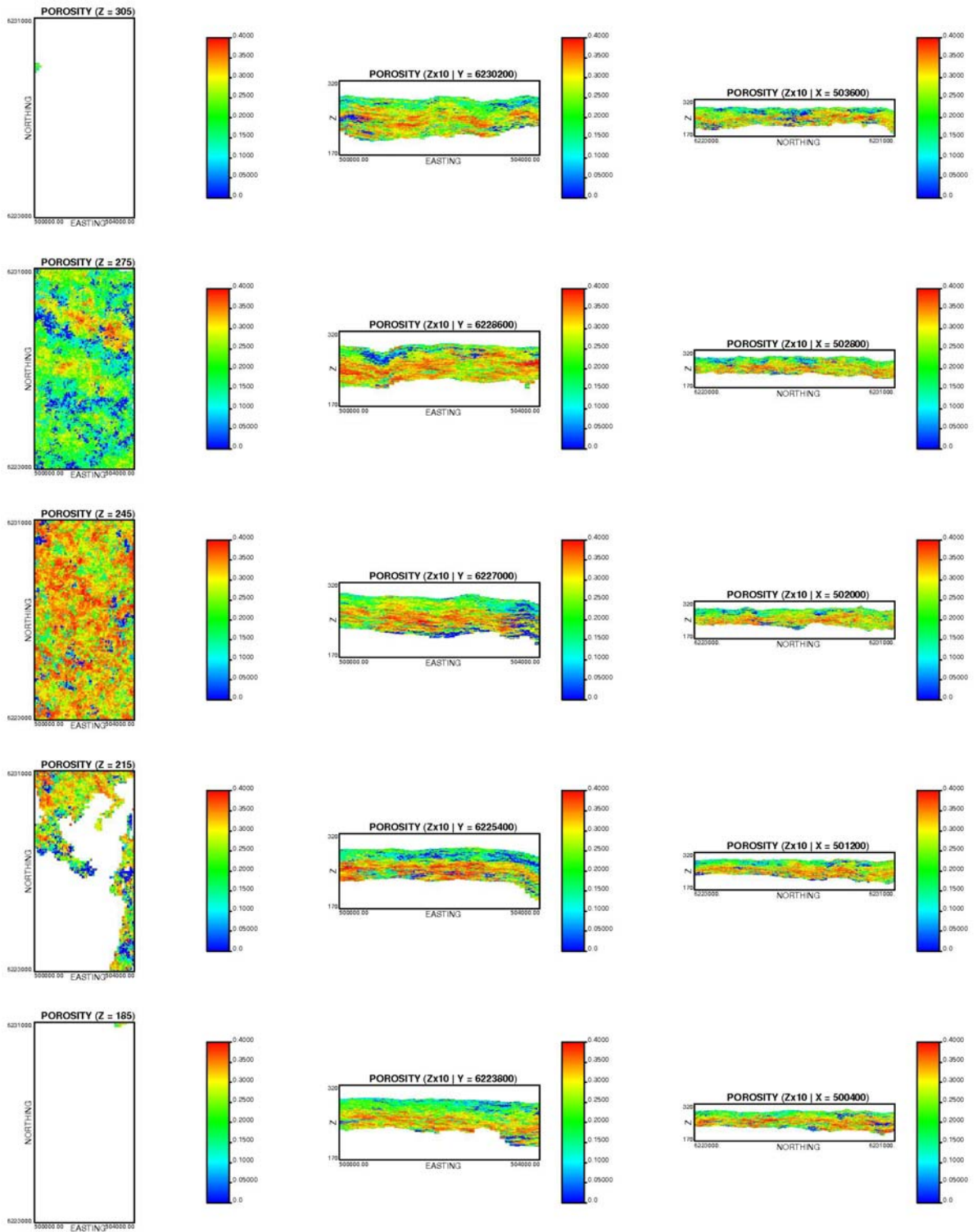


**Figure 13:** Cross sections through the first porosity realization.

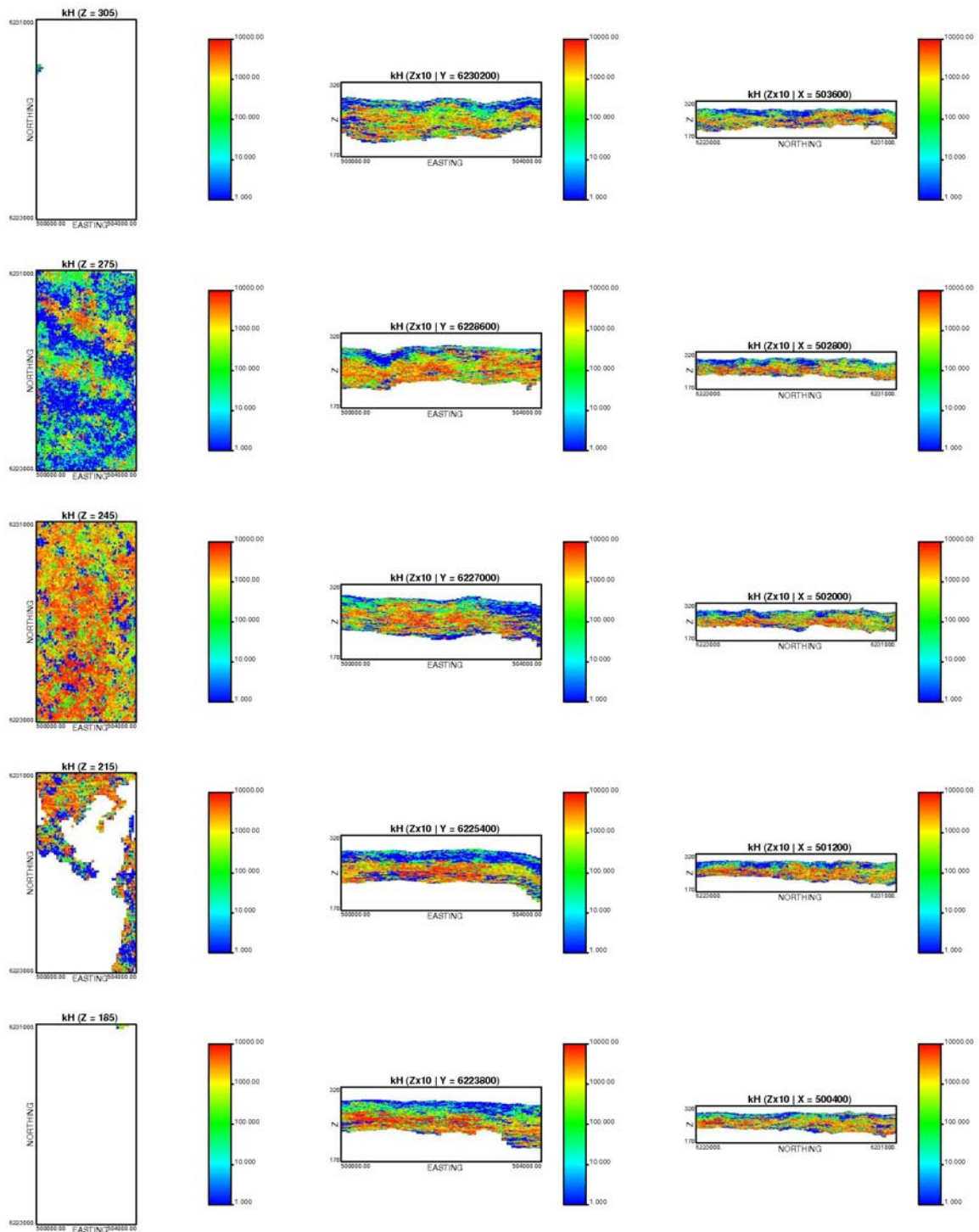


**Figure 14:** Cross sections through the first horizontal permeability realization.

## SAGD Flow Sensitivity

A small sensitivity study is setup to illustrate the importance of adopting a particular permeability methodology. CMG STARS is used for the flow simulations. A simple input deck is considered. A network of 20 x 2 x 2m sized Cartesian flow simulation blocks are used within a 1000 x 200 x 100m southwest subset of the model area in Figure 2 for a total of 40 x 100 x 50 (200,000) blocks in the  $X$ ,  $Y$ ,  $Z$  directions, respectively. There is a single injector-producer well pair 500m in length located approximately 6m from the bottom of the reservoir. The project duration is 114 months (9.5 years) with 6 months initial hot finger circulation. The component, rock-fluid properties, and initial conditions are standard for the McMurray Formation.

Some preliminary steps are performed within the drainage volume before implementing SAGD flow simulation. The first step is extracting the closest facies,  $\phi$ ,  $S_w$ ,  $k_H$ ,  $k_V$ , and  $k_V:k_H$  variables from the geological grid to each of the 200,000 flow simulation grid cells. The extracted geology is then used to downscale to a fine scale 1.0 x 1.0 x 0.5m grid network. A re-simulation procedure (sequential indicator simulation for facies and sequential Gaussian simulation for  $\phi$ ,  $S_w$ ,  $k_H$ ,  $k_V$ , and  $k_V:k_H$ ) conditioned by the extracted geology and variography is used for the downscaling. It is the geology at this fine scale that is used for flow simulation.

Four different flow simulation runs are illustrated in this work: (1) using the  $k_H$  and  $k_V$  models generated by the proposed permeability mini-model approach as input, (2) using the simple quadratic by-facies relationships in Figure 12 (blue) as input (3) using constant homogeneous  $k_H$  and  $k_V$  within each facies, and (4) using, in addition to constant  $k_H$  and  $k_V$  distributions, constant  $\phi$  and  $S_w$ . All the geological variables for extraction and downscaling are derived from the first geostatistical realization. Other sensitivity runs were performed dealing with different downscaling and upscaling methodologies; however, it is the sensitivity of the flow simulation results to only the permeability modeling methodology that is attempting to be captured in this work.

The steam chamber (100°C iso-surface) for the recommended mini-model permeability modeling methodology is shown during the hot finger circulation startup (June 2005), the high pressure phase (June 2007), the low pressure phase (June 2010) and the blowdown phase (June 2013) in Figure 15. The porosity model is superimposed. Notice the rising roughly cone-shaped steam chamber growth with time and increasing porosity. Figure 16 shows the output COP, IOR, CSOR, and CWI results using the recommended approach (solid black lines), the quadratic approach (broken red lines), the homogenous  $k_H$  and  $k_V$  approach (broken yellow lines) and homogenous  $k_H$ ,  $k_V$ ,  $\phi$ , and  $S_w$  (broken blue lines). The different permeability modeling approaches certainly produce different flow results.

It is difficult in this setting to determine the best permeability methodology. In practice, some flow history would be required. The best permeability modeling methodology for that particular setting would then be the one producing the best history match. Here, our observations must be limited to the conclusion that the permeability modeling methodology is a significant decision made for any project.

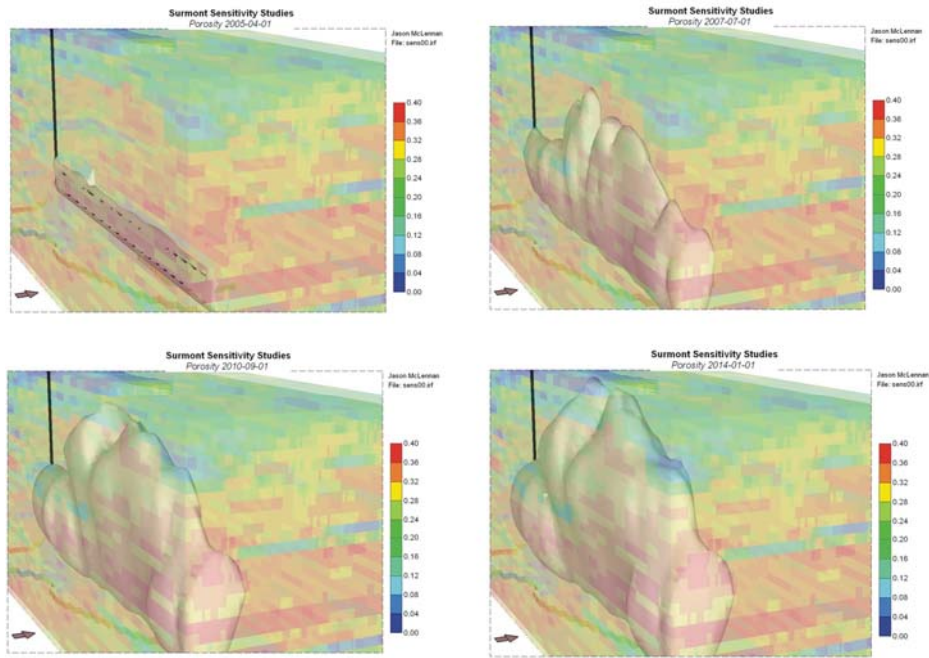


**Figure 15:** The steam chamber during the startup (top left), high pressure (top right), low pressure (bottom left), and blowdown (bottom right) phases of operation. The porosity model is transparently superimposed.

### Permeability Modeling Methodology

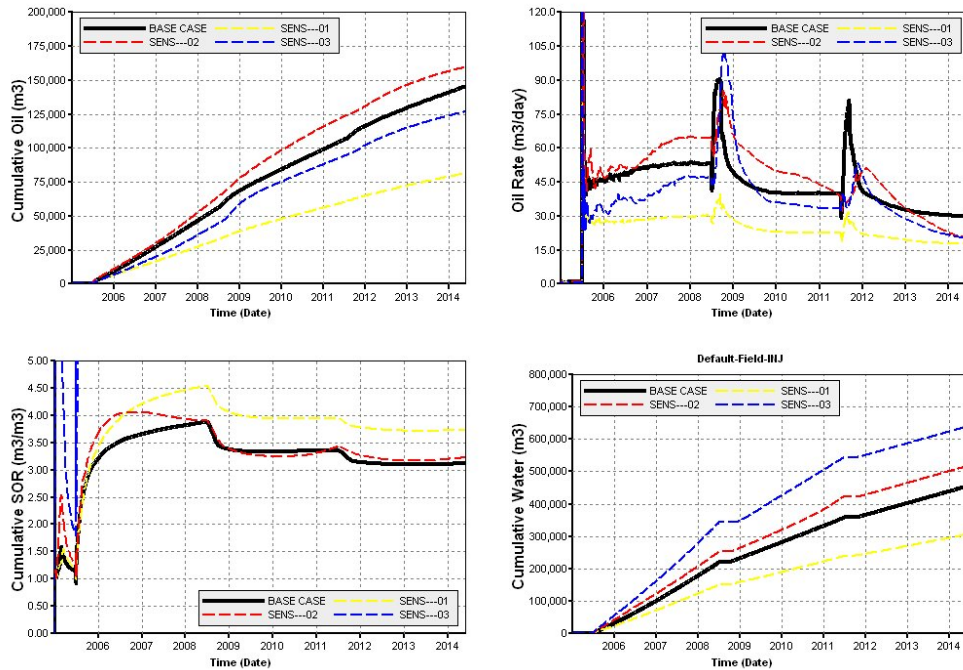


**Figure 16:** The COP, IOR, CSOR, and CWI SAGD production performance profiles for the permeability methodology sensitivity studies.

## Conclusions

- There are three main challenges associated with permeability modeling: (1) limited core permeability measurements random porosity-permeability scatters, (2) core expansion and preferential core sampling bias, and (3) vastly different scales between core plug samples, geological grid cells, and flow simulation grid cells.
- The proposed mini-modeling approach overcomes these challenges within a relatively straightforward mini-model and flow simulation framework.
- The difference between more traditional and the proposed permeability modeling methodology in terms of SAGD flow simulation results is significant.

## Acknowledgements

The authors would like to thank the sponsors for the CCG (Center for Computational Geostatistics) as well as NSERC for their support.

## References

- [1] Butler, R. *SAGD Comes of AGE!*, Journal of Canadian Petroleum Technology, 37(7):9-12, 1998.
- [2] Butler, R. *Thermal Recovery of Oil and Bitumen*, GravDrain Inc., Calgary, Alberta, 2004.
- [3] Alberta Energy and Utilities Board. *Alberta's Reserves 2004 and Supply/Demand Outlook 2005-2014*, September 2005.
- [4] Moritis, G. *Oil Sands Drive Canada's Production Growth*, Oil and Gas Journal, June 7, 2004.
- [5] Computer Modeling Group Ltd., #150 3553-31 Street NW, Calgary, Alberta, T2L 2K7. *STARS Software*. www.cmgl.ca.
- [6] Deutsch, C., Dembicki, E. and Yeung, K. *Geostatistical Determination of Production Uncertainty: Application to Firebag Project*, Center for Computational Geostatistics (CCG), University of Alberta, Canada, 2002.
- [7] Deutsch, C. *Geostatistical Reservoir Modeling*. Oxford University Press, 2002.
- [8] McLennan, J. A. *Scaling and Gridding Geology for SAGD Flow Simulation*. Center for Computational Geostatistics (CCG), University of Alberta, Canada, 2005.
- [9] Donnelly, J. and Hitchner, J. *Determining Oilsand Reservoir Properties from Logs and Core – The Controversy Continues*. SPE (CIM/CHOA) Paper 79034.
- [10] Zwicky, R. and Eade, J. *The Tar Sand Core Analysis Versus Log Analysis Controversy – Does it Really Matter*. The Oilsands of Canada-Venezuela, CIM Special Volume 17, 1977.
- [11] Waite, M., Johansen, S., Betancourt, D., and Acharya, U. *Modeling of Scale-Dependent Permeability Using Single Well Micro-Models: Application to Hamaca Field, Venezuela*. SPE Paper 86976.